Advanced Synthesis & Catalysis

ADVANCED SYNTHESIS & CATALYSIS
advsynthcatal.com

RESEARCH ARTICLE OPEN ACCESS

Enzyme–MOF Composites: Quantitative Benchmarking and Evaluation of Biocatalyst Performance

Annika J. Weber[1] | Maria Alessandra Martini[1] | Esther Mittmann[1] | Hannah P. Seufert[1] | Marc F. Münker[1] | Ilona Wagner[2] | Emily Bevier[2] | Manuel Tsotsalas[2] | Christof M. Niemeyer[1] | Kersten S. Rabe[1]

[1]Institute for Biological Interfaces 1 (IBG1), Karlsruhe Institute of Technology (KIT), Eggenstein-Leopoldshafen, Germany | [2]Institute of Functional Interfaces (IFG), Karlsruhe Institute of Technology (KIT), Eggenstein-Leopoldshafen, Germany

Correspondence: Kersten S. Rabe (kersten.rabe@kit.edu)

Received: 2 February 2026 | **Revised:** 6 May 2026 | **Accepted:** 8 June 2026

Keywords: biocatalysis | characterization | enzyme immobilization | metal–organic frameworks (MOFs) | stability

ABSTRACT

The integration of enzymes into crystalline framework materials offers a promising route to combine the selectivity of biocatalysis with the practical advantages of heterogeneous catalysts. In this work, we present a quantitative benchmarking study of enzyme immobilization within the calcium benzene-1,4-dicarboxylate (CaBDC) metal–organic framework (MOF) using two structurally and functionally distinct model enzymes: phenolic acid decarboxylase (PAD) and cytochrome c (CC). An in situ synthesis route enabled the formation of enzyme@CaBDC composites under mild aqueous conditions. We establish rigorous and transparent evaluation practices for enzyme@MOF systems, with particular emphasis on reliable determination of enzyme loading and activity. Quantitative analyses show that encapsulation preserves biocatalytic activity but that apparent reaction rates are frequently limited by substrate accessibility and mass-transport effects. Immobilization in CaBDC does not improve the intrinsic thermal or solvent stability of the already robust enzymes studied here. However, it successfully converts soluble biocatalysts into recoverable solid formulations that facilitate reuse. Immobilization of pre-reduced CC yielded catalytically active ^{red}CC@CaBDC composites enabling carbene-transfer reactions in non-aqueous media. Overall, this work provides a methodological template for the quantitative assessment of enzyme@MOF composites and highlights key limitations that must be considered when interpreting immobilization effects and comparing different systems.

1 | Introduction

Immobilization of enzymes is a cornerstone technology in industrial biotransformations, offering enhanced stability, reusability, and process control [1–8]. This can be achieved through several strategies, including (i) support-bound immobilization, where enzymes are covalently or noncovalently attached to solid carriers [9–17], (ii) encapsulation, which involves entrapping enzymes within semipermeable matrices [11, 18–20], and (iii) self-immobilization, where enzymes form aggregates or cross-linked networks without the need for external supports [12, 21–29, 30]. Each of these advanced approaches offers distinct advantages, enabling the fine-tuning of biocatalytic performance and driving innovation across the landscape of industrial biotechnology [1, 3, 5, 31].

Recently, enzyme immobilization in metal–organic frameworks (MOFs) and other crystalline framework materials has attracted growing attention, as combining the precision of biological catalysis with the robustness of materials science offers significant promise for sustainable chemistry [32–34]. MOFs are highly porous crystalline materials composed of metal ions coordinated to organic ligands, providing exceptional surface areas and tunable architectures suitable for diverse applications [32, 35, 36, 37]. Leveraging these unique properties, the encapsulation of enzymes within the rigid MOF lattice has emerged as a powerful

strategy to enhance enzymatic stability against denaturing reagents and harsh reaction conditions [38–44, 45]. The immobilization of enzymes within MOFs can generally be achieved through two main approaches: (i) in situ encapsulation, where the enzyme is present during MOF formation and becomes entrapped within the porous matrix, and (ii) post-synthetic loading, where the enzyme is introduced into a preformed MOF and either infiltrates its pores or binds to its surface [38, 46]. Because the in situ strategy allows the inclusion of enzymes of diverse molecular sizes without being constrained by the intrinsic pore dimensions, this approach was chosen for the present study. For a straightforward one-pot synthesis of enzyme@MOF composites, the reaction conditions must preserve enzymatic activity and structural integrity. Consequently, MOFs that can crystallize under mild, aqueous conditions are particularly advantageous.

Benchmarking enzyme@MOF composites across the literature remains challenging due to the lack of standardized experimental design and reporting practices, particularly with respect to catalyst loading [38]. Although the synthesis of enzyme@MOF composites and the influence of various parameters have been extensively reviewed [38], this work showcases an experimental approach that is easy to implement and that allows for robust systematic and critical evaluation of enzyme@MOF performance. In this work, our primary objective was not to demonstrate improved catalytic activity or stability upon immobilization but to establish a transparent and rigorous approach for the quantitative evaluation of enzyme@MOF systems. Several prior studies have reported enhanced performance, yet such claims are often difficult to evaluate due to incomplete or inconsistent quantification of the enzyme content within the MOF. By placing particular emphasis on reliable enzyme quantification and direct soluble versus immobilized benchmarking, we aim to provide a methodological template that enables meaningful interpretation of apparent activity and stability. This evaluation-focused approach is intended to support more robust and comparable assessment of enzyme@MOF composites and to identify genuine functional advantages as opposed to artifacts arising from diffusion limitations or framework instability. Guided by prior studies and preliminary assessments of enzyme compatibility, we selected the metal–organic framework CaBDC (calcium benzene-1,4-dicarboxylate, or terephthalate trihydrate) [47], which has been successfully employed in several enzyme immobilization studies [48–50].

The objective of this study is to demonstrate the effective immobilization of two structurally and functionally distinct enzymes in CaBDC: the 44 kDa phenolic acid decarboxylase (PAD) from *Enterobacter* sp. [51] and the 15 kDa cytochrome c (CC) from *Rhodothermus marinus* [52] which was recently engineered to form nonnatural silicon–carbon bonds. These two enzymes represent unrelated catalytic classes and differ markedly in molecular size and structure (Figure 1). PAD is a homodimeric enzyme belonging to the phenolic acid decarboxylase superfamily and features a solvent-exposed catalytic pocket formed by a half-open β-barrel architecture [53], enabling direct substrate access from the surrounding aqueous phase. In contrast, CC is a compact, predominantly α-helical monoheme protein [54] whose catalytic activity in carbene-transfer reactions originates from an iron–porphyrin active site that is deeply embedded within the protein fold and accessible only through a narrow substrate channel. Directed evolution has reshaped the immediate heme environment and neighboring amino-acid residues to stabilize reactive iron–carbene intermediates and control stereoselectivity in non–native bond-forming reactions. The pronounced differences in molecular size, fold, active-site accessibility, and catalytic mechanism between PAD and CC make them a complementary model pair for assessing how enzyme architecture and active-site exposure influence immobilization efficiency, substrate diffusion, and apparent catalytic performance in enzyme@MOF composites. Comprehensive physicochemical and functional characterization, as performed in this study, enables a systematic assessment of whether CaBDC-based immobilization offers advantages over soluble enzymes or alternative immobilization methods.

2 | Results and Discussion

As CC originates from a thermohalophilic bacterium and has been shown to remain folded under challenging conditions such as elevated temperatures and catalytically competent under non-native, chemically demanding reaction conditions [52], we focused initially on the potentially less robust PAD to identify incompatibilities between enzymes and MOF synthesis conditions. Consequently, we first attempted to immobilize PAD using several MOF systems frequently reported in the literature for enzyme encapsulation, namely ZIF-8 [55–57], ZIF-90 [58–60], and MIL-53 [61–63]. However, in all cases, the high concentrations of linker or metal ions required for MOF formation adversely affected enzymatic activity (Figure S1a–c). This observation underscores that no universal MOF platform can accommodate all enzymes equally well and is in line with reported data [37] and highlights the necessity of carefully screening both materials and synthesis conditions for compatibility with the specific enzyme prior to immobilization. In the case of PAD, both $CaCl_2$ and Na_2BDC were found to have little to no detrimental effect on enzymatic activity (Figure S1d), even at concentrations

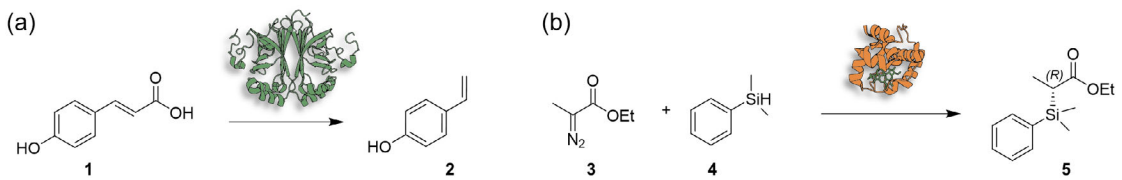

FIGURE 1 | The two enzymes used in this study for MOF encapsulation catalyze fundamentally different classes of reactions. (a) *Phenolic acid decarboxylase* (PAD, green; PDB: 4UU3 [53]) catalyzes the nonoxidative decarboxylation of *p*-coumaric acid (**1**) to form 4-vinylphenol (**2**), while (b) *cytochrome c* (CC, orange; PDB: 6CUK [54]) catalyzes the formation of an organosilicon compound (**5**) from ethyl 2-diazopropanoate (**3**) and phenyl dimethylsilane (**4**).

exceeding those employed during CaBDC synthesis in our study. We recommend that such investigations should be considered as an initial step for enzyme@MOF immobilization studies.

2.1 | Immobilization of Enzymes in CaBDC-MOF (Enzyme@CaBDC)

The metal–organic framework CaBDC is composed of calcium cations (Ca^{2+}) coordinated to terephthalate (BDC) linker molecules (Figure 2a) [47, 50]. Crystallization of CaBDC without enzymes was achieved by combining aqueous solutions of calcium chloride ($CaCl_2$) and disodium terephthalate (Na_2BDC), each at a final concentration of 300 mM following adaptations of previously reported procedures [48–50]. After 16 h of incubation, the resulting precipitate was collected, thoroughly washed with water, and dried to yield a fine white powder (Figure 2b). Microscopic analysis revealed a distinctive butterfly-like crystal morphology characteristic of CaBDC in this study (Figure 2c).

For their immobilization in CaBDC-MOF, both PAD and CC were produced and purified as previously described (Figure S2) [16, 17, 25, 52]. PAD (final concentration of 50 µM) was added to 300 mM Na_2BDC and MOF formation was initiated by the addition of 300 mM $CaCl_2$ (Figure 2d). PAD@CaBDC was obtained as a white power (Figure 2e) formed by butterfly-like crystals (Figure 2f) as observed for the pure MOF (Figure 2c). The same synthesis was also performed for CC (Figure 2g) and here the resulting CC@CaBDC emerged as an orange powder after drying (Figure 2h), retaining the crystals shape as observed in the other cases (Figure 2i). The characteristic crystallinity of the CaBDC-MOF was verified by X-ray diffraction (XRD) for the synthesized pure CaBDC, PAD@CaBDC and CC@CaBDC (Figure S3). In contrast, reducing the concentrations of $CaCl_2$ or Na_2BDC while maintaining a constant enzyme concentration resulted in CC@CaBDC crystals with less defined morphology (Figure S4).

2.2 | Quantification of Enzymes in CaBDC-MOF

Quantifying the amount of enzyme immobilized within a MOF is essential to enable meaningful comparisons across different MOF formulations and to evaluate their respective efficiencies in enzyme loading and activity retention. One key performance parameter is the protein loading, defined as the ratio of the mass of immobilized enzyme to the mass of the carrier material [38]. However, direct spectrophotometric quantification of enzymes such as PAD based on its intrinsic absorption at 280 nm is not feasible, as the terephthalate linker (BDC^{2-}) exhibits strong absorbance at the same wavelength. While PAD can be effectively released from the framework by dissolving the CaBDC-MOF in 0.5 M ethylenediaminetetraacetic acid (EDTA) (Figure 3a) [64, 65], the EDTA remaining in solution also interferes with UV–Vis absorption measurements at 280 nm, rendering direct quantification unreliable. Accordingly, the enzyme content within CaBDC was determined after framework dissolution by SDS–PAGE followed by densitometric (gray-scale) analysis (Figure 3b). The PAD band intensity obtained after MOF dissolution was compared with calibration samples containing defined amounts of PAD, allowing accurate quantification of the encapsulated protein. Using this method, we determined that $160 \pm 21\ pmol_{PAD}/mg_{PAD@CaBDC}$ ($3.5 \pm 0.5\ \mu g_{PAD}/mg_{PAD@CaBDC}$) were incorporated when using a synthesis solution containing 50 µM PAD, corresponding to a loading efficiency of 19%. Note that the quantified enzyme amounts include both PAD encapsulated within the lattice and PAD that is strongly bound

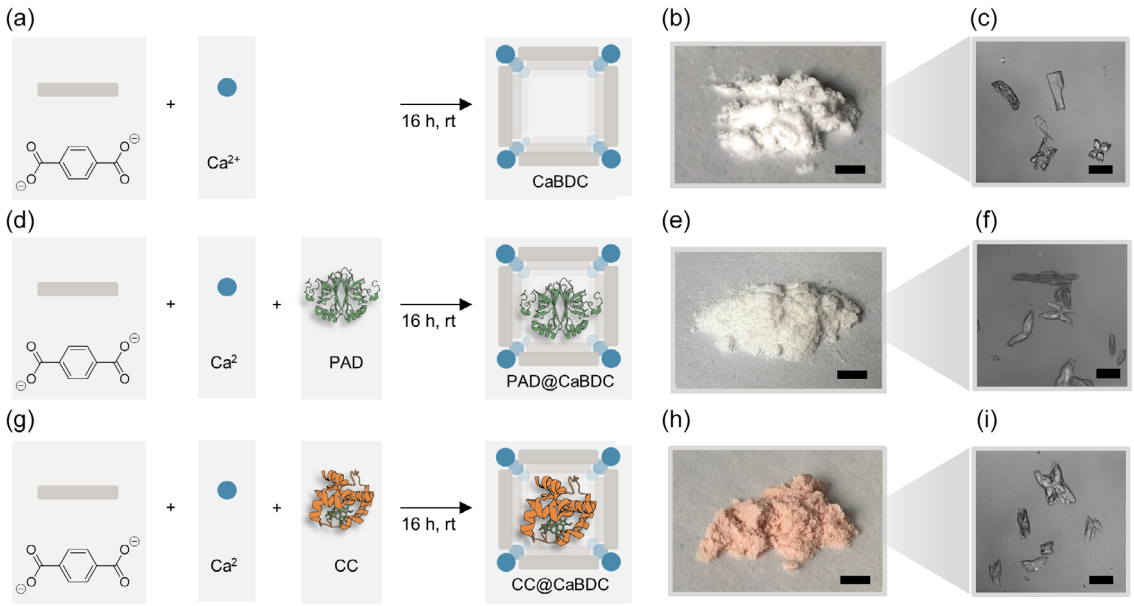

FIGURE 2 | Preparation of CaBDC-MOF and immobilization of PAD and CC in CaBDC-MOF. (a) Crystallization of terephthalate (gray bar, BDC) and calcium cations (Ca^{2+}, blue circle) to form CaBDC. (b) Resulting crystalline white powder of CaBDC. (c) Microscopic image of CaBDC crystals. (d) In situ synthesis of PAD@CaBDC. (e) Resulting crystalline white powder of PAD@CaBDC. (f) Microscopic image of PAD@CaBDC crystals. (g) In situ synthesis of CC@CaBDC. (h) Resulting crystalline redish powder of CC@CaBDC. (i) Microscopic image of CC@CaBDC crystals. Scale bar for (b), (e), (h): 0.5 cm. Scale bar for (c), (f), (h): 50 µm.

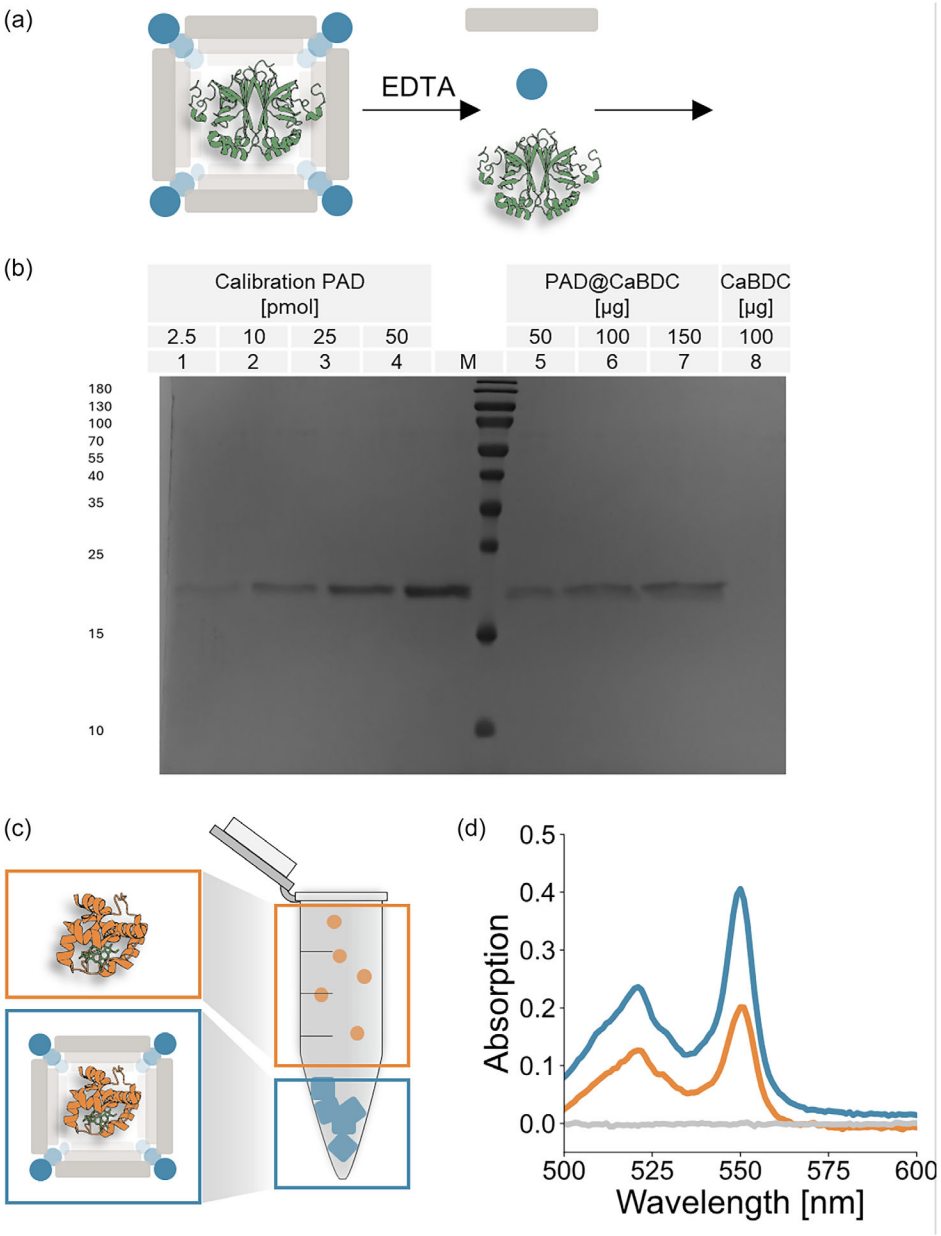

FIGURE 3 | Quantification of enzyme@CaBDC (a) The amount of enzyme immobilized in CaBDC can be directly determined by dissolving the MOF with EDTA (0.5 M, pH 8) and thus re-solubilizing the enzymes, enabling the direct determination of the amount of protein in solution. (b) SDS-PAGE with subsequent Coomassie staining of defined amounts of PAD (lanes 1–4, 2.5, 10, 25, 50 pmol) as well as PAD@CaBDC (lanes 5–7, 50, 100, and 150 µg) dissolved with EDTA. Based on gray scale analysis of the intensity of the bands the amount of PAD immobilized in PAD@BDC was calculated. Note that CaBDC (lane 8) does not result in any bands. (c) CC can also be quantified via the established ferrous assay, which can be applied to the CC remaining in the supernatant after synthesis (orange box) as well as to CC released by EDTA from the CC@CaBDC MOF (blue box). (d) UV–Vis spectra of CC remaining in the supernatant after synthesis (orange) as well as released by EDTA from the CC@CaBDC MOF (blue), The characteristic absorption band at 550 nm was used to quantify CC. Note, that soluble Ca^{2+}, BDC^{2-}, and EDTA do not absorb in this wavelength range (gray).

to the surface and was not removed during the intensive washing procedure following the in situ PAD@CaBDC synthesis.

While the quantification strategy described here is broadly transferable to any protein, several complementary methods to estimate enzyme loading, including protein depletion from supernatants, are available that may be advantageous in specific cases, including colorimetric protein quantification assays (e.g., Bicinchoninic Acid, BCA), thermogravimetric analysis (TGA), inductively coupled plasma mass spectrometry (ICP–MS), or absorption spectroscopy [42, 55, 66]. However, these typically report only the total protein content and may suffer from system-specific limitations, such as interference by MOF components or reliance on enzyme-specific labels that can alter catalytic behavior. In contrast, the approach presented here enables selective quantification of the target protein following framework dissolution, distinguishing it from other potential protein impurities. This specificity is particularly valuable for commercial enzyme preparations, which often exhibit variable purity, and allows accurate loading determination irrespective of enzyme

class, size, or cofactor requirement. In this context, PAD and CC serve as illustrative case studies demonstrating how enzyme-appropriate loading-determination strategies can be selected based on general physicochemical properties, rather than as limitations to the generality of the evaluation approach.

For enzymes containing chromophoric cofactors with characteristic absorption bands at longer wavelengths, additional spectroscopic techniques can provide direct and selective quantification. In this study, we compared three simple and robust approaches to determine the loading of the heme-containing enzyme cytochrome c (CC) immobilized in CaBDC. As in the case of PAD, SDS–PAGE followed by densitometric analysis was initially applied to evaluate the previously described quantification approach. This yielded a loading of 516 ± 137 $pmol_{CC}/mg_{CC@CaBDC}$ (7.6 ± 2.0 $\mu g_{CC}/mg_{CC@CaBDC}$) (Figure S5). In addition, two independent methods based on the heme-specific ferrous assay were developed (Figure 3c) [52]. In the first approach, CC was released from the MOF by dissolving CaBDC with 0.5 M EDTA [64, 65], allowing direct quantification via the reduced heme cofactor's characteristic absorption upon addition of sodium dithionite (NaDT). From this measurement, a loading of 474 ± 142 $pmol_{CC}/mg_{CC@CaBDC}$ (7.0 ± 2.1 $\mu g_{CC}/mg_{CC@CaBDC}$) (Figure 3d, blue trace). Control experiments confirmed that Ca^{2+}, BDC, and EDTA did not absorb in this spectral range (Figure 3d, gray trace). Likewise, quantification of unincorporated CC remaining in the supernatant after synthesis using the same ferrous assay yielded 462 ± 70 $pmol_{CC}/mg_{CC@CaBDC}$ (6.8 ± 1.0 $\mu g_{CC}/mg_{CC@CaBDC}$) (Figure 3d, orange trace). The results from all three methods were in excellent agreement, and the averaged value of 484 ± 97 $pmol_{CC}/mg_{CC@CaBDC}$ and 7.1 ± 1.4 $\mu g_{CC}/mg_{CC@CaBDC}$ was used to calculate an immobilization efficiency of 66%. These complementary approaches not only reinforce the reliability of the quantification but also lay the groundwork for transferable benchmarks and standardized metrics. Their applicability to other heme- or chromophore-containing enzymes positions them as valuable contributions toward meaningful and consistent evaluation of enzyme@MOF composites in functional biocatalyst design.

Under identical synthesis conditions, CaBDC incorporated more than twice the molar amount of CC compared to PAD. The markedly distinct molecular dimensions of the two enzymes (the monomeric CC, with a molecular weight of approximately 15 kDa versus PAD, with a monomeric mass of 22 kDa forming a 44 kDa homodimer) as well as surface properties such as charge distribution and hydrophobicity are expected to contribute to the observed encapsulation efficiency. The total amount of enzyme immobilized is expected to be increased by raising the enzyme concentration used during the MOF synthesis. Increasing the enzyme concentration fourfold led to the expected formation of butterfly-like crystals and the corresponding XRD pattern characteristic of CaBDC under higher absolute protein loadings (414 ± 115 $pmol_{PAD}/mg_{PAD@CaBDC}$ and 1392 ± 18 $pmol_{CC}/mg_{CC@CaBDC}$) but resulted in reduced loading efficiencies of 12% and 36%, respectively, as determined by SDS–PAGE and gray-scale analysis (Figure S6).

This trade-off between absolute loading and immobilization efficiency highlights the importance of tailoring synthesis conditions to balance enzyme utilization and performance. Given that PAD can be recombinantly produced and purified at high yields exceeding 100 milligrams per liter of bacterial culture [25], higher enzyme concentrations during synthesis but lower loading efficiency may be acceptable, whereas for low-yield enzymes such as 14 milligrams per liter of bacterial culture for CC, a lower enzyme concentration is more resource-efficient. Therefore, all subsequent encapsulation experiments were performed at 50 μM enzyme concentration to enable consistent and comparable analysis of both systems.

2.3 | Biocatalytic Reactions Employing Enzyme@CaBDC in Aqueous Buffers

With the quantification of immobilized enzyme in CaBDC established, the catalytic activities of the resulting biocatalysts could be quantitatively assessed. The activity of PAD@CaBDC was investigated via the conversion of p-coumaric acid (**1**) to 4-vinylphenol (**2**) (Figure 1a) using established HPLC analytics (Figure S7) [30]. To evaluate the influence of immobilization, equal amounts of PAD were compared in their soluble and immobilized forms. The soluble enzyme catalyzed the reaction at a higher initial rate, which can be attributed to mass transfer limitations in PAD@CaBDC arising from substrate diffusion through the MOF structure and restricted accessibility of encapsulated enzyme molecules. Nevertheless, the final product concentrations achieved by PAD@CaBDC were comparable to those of the soluble enzyme (Figure 4a), demonstrating that while diffusion limits the reaction rate, catalytic turnover remains largely preserved within the MOF.

The catalytic activity of CC was assessed using the reported reaction between the diazo ester **3** and the silane **4** to yield the organosilicon compound (**5**) (Figure 1b) using established GC and chiral HPLC analytics (Figure S8) [16, 52]. When this reaction was performed in the commonly used phosphate buffer (PB, 50 mM sodium phosphates) [16, 17, 52], a pronounced destabilization of CC@CaBDC was observed, evidenced by pH changes and an increase in dissolved BDC in the supernatant (Figure S9) [48]. In contrast, incubation of CaBDC in the nonphosphate HEPES buffer (50 mM, pH 7.4) resulted in only minor variations in pH and BDC concentration over time. Consequently, HEPES buffer was employed for all subsequent biocatalytic reactions involving CaBDC. Despite its stability in HEPES buffer, a slight dissolution of CaBDC cannot be fully excluded, and the release of CC may contribute to the overall product formation observed in solution. Phosphate containing buffers are widely recognized for promoting degradation of metal organic frameworks. However, it is often overlooked that even alternative buffer systems can have a mild destabilizing effect on frameworks such as CaBDC [67]. This is particularly relevant when individual framework components are sufficiently soluble in water to partially equilibrate under aqueous reaction conditions. As a consequence, the observed activity must be interpreted as an apparent catalytic performance that may arise from a combination of true heterogeneous catalysis by intact, immobilized and accessible enzymes and homogeneous catalysis by intact enzyme released upon partial framework dissolution. It is therefore essential to evaluate MOF stability under the exact conditions employed for enzymatic activity measurements, as framework dissolution can otherwise result in substrate conversion by the soluble enzyme

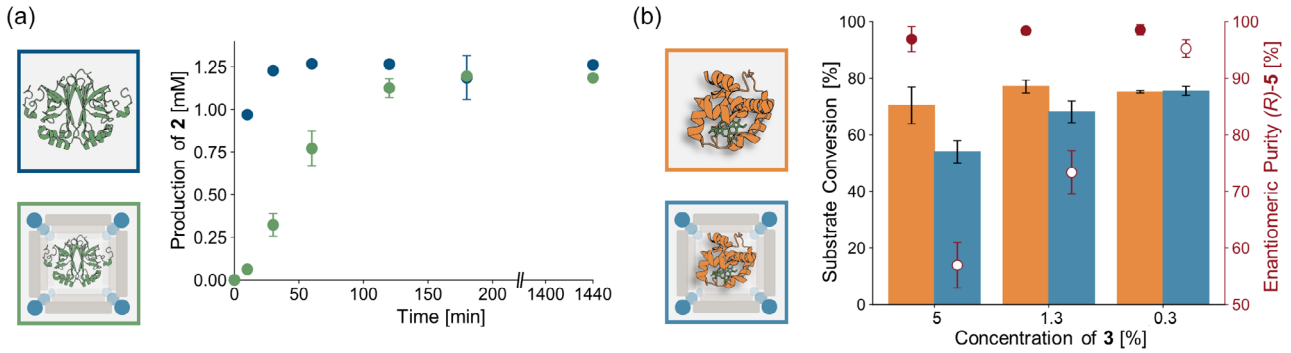

FIGURE 4 | Activity of PAD@CaBDC and CC@CaBDC compared to soluble PAD and CC respectively. (a) Formation of **2** in batch reactions using 0.2 μM (in regard to the PAD amount) each of PAD (blue) or PAD@CaBDC (green) and 1.25 mM **1** in HEPES buffer (50 mM, pH 7.4). The reaction was monitored at selected time points over the course of 24 h. (b) Substrate conversion (bars) and enantiomeric purity of product **5** (circles) in batch reactions using 5 μM (in regard to the CC amount) each of CC (orange) and CC@CaBDC (blue) with varying concentrations of substrate **3** (5, 1.3, 0.3 mM), 10 mM **4** and NaDT in HEPES buffer for 4 h under anaerobic conditions. Error bars represent the standard deviation from duplicates.

fraction rather than exclusively by the intended enzyme@MOF system. To minimize this risk, adding soluble components of the MOF, particularly the corresponding salt, could help to stabilize the structure of the MOF and reduce its dissolution under reaction conditions [48–50].

When comparing equal total amounts of CC biocatalyst, either as soluble enzyme or immobilized as CC@CaBDC, we also investigated the effect of varying concentrations of the diazo substrate **3** (5, 1.3, and 0.3 mM) while maintaining a fixed excess of silane **4** at 10 mM to favor rapid conversion of **3**, as this is critical to achieve high enantioselectivity of the reaction [17]. Substrate conversion was calculated based on the concentration of **3**, as it represents the limiting reagent. Soluble CC achieved conversions exceeding 70% and maintained high enantiomeric purity of product **5** (>95%) under all tested conditions. In contrast, while CC@CaBDC afforded comparable conversions and enantiomeric purity at the lowest substrate concentration (0.3 mM **3**), increasing the concentration of **3** resulted in a decline in catalytic performance, with enantiomeric purity dropping to 57% at 5 mM **3**.

These trends suggest that not all CC molecules immobilized within CaBDC participate in catalysis, consistent with previous observations that a low effective CC-to-**3** ratio leads to diminished enantioselectivity [17]. We had hypothesized that encapsulating CC within a MOF lattice might mitigate substrate-induced conformational changes known to occur upon exposure to diazo esters [17], thereby enhancing tolerance toward higher substrate concentrations. However, this was not observed, suggesting that only CC molecules located near the outer surfaces or accessible pores of CaBDC contribute significantly to catalysis, while those embedded deeper within the lattice are likely inaccessible due to mass transport limitations. The immobilized materials likely comprise a heterogeneous population of lattice-embedded, defect-associated, and surface-adsorbed enzymes. CaBDC forms layered structures with one-dimensional channels and interlayer spacings in the angström to sub-nanometer range [47], which are substantially smaller than the hydrodynamic dimensions of intact enzymes such as CC or PAD dimers [51–54]. In dense carrier materials, substrate concentration is expected to decrease from the surface toward the core due to transport limitations, such that catalysis is predominantly governed by enzymes located near the external surface or within more accessible defects. Additionally, structural perturbations of CC arising from altered microenvironments cannot be excluded and may influence the apparent activity. As a result, high enantiomeric purity can only be maintained at lower substrate concentrations compared to previously reported particle-immobilized CC systems [17]. Furthermore, given the partial dissolution of CaBDC under reaction conditions, it remains possible that catalysis is predominantly driven by CC molecules released from the framework, with limited or no direct substrate diffusion into the intact MOF structure.

In summary, these results illustrate that only a detailed, quantitative comparison between soluble and MOF-immobilized enzymes reveals the complex interplay between mass transport, structural accessibility, and catalytic performance. Such analyses are essential to understand how immobilization affects enzyme function and to guide the rational optimization of biocatalysts for practical applications. The in situ synthesis approach, frequently described as straightforward in the literature, proved to be easily applicable for PAD and CC in CaBDC. The resulting composites retained catalytic activity, confirming that enzyme immobilization in CaBDC is generally compatible with enzymes of different sizes and reaction classes. In order to apply enzyme@MOF formulations in biocatalytic reactions, precise quantification of the amount of enzyme encapsulated inside the MOF is essential. Gel analysis after MOF dissolution enables selective detection of virtually any protein enzyme by SDS–PAGE, allowing precise quantification of the enzyme of interest irrespective of its catalytic class, cofactor requirement, or the presence of inorganic framework residues and other impurities. Furthermore, for enzymes containing chromophores, such as the heme-specific detection of CC shown here, alternative quantification methods allowing acceleration and accuracy become feasible. Building on these insights, we next examined the stability of CaBDC-encapsulated enzyme materials under different process conditions.

2.4 | Stability of Enzyme@CaBDC under Different Process Conditions

Encapsulation of enzymes in MOFs has often been reported to enhance stability against heat, mechanical stress, or exposure

to organic solvents [38, 41–44]. To evaluate whether such effects apply to PAD@CaBDC, we first examined its solvent tolerance. A phenolic acid decarboxylase related to the PAD used in this study has previously been reported to retain activity in certain organic solvents, including wet esters such as CPME (cyclopentyl methyl ether) and MTBE (methyl *tert*-butyl ether) [68]. To assess whether immobilization in CaBDC influences solvent tolerance, equal amounts of PAD, formulated either as PAD@CaBDC or as lyophilized enzyme, were tested in a biphasic MTBE/HEPES buffer system (Figure S10). Both forms catalyzed the conversion of p-coumaric acid (**1**) to 4-vinylphenol (**2**), but the lyophilized enzyme showed higher activity than PAD@CaBDC. Solvent stability was further examined by incubating both formulations in various organic solvents for 5 days (Figure 5a). Three solvents with different hydrophilicities were selected based on their log *p* values [69]. Acetonitrile (MeCN, log $p > 0$) is fully miscible with water, MTBE (log $p < 2$) is partially miscible, and cyclohexane (CH, log $p > 2$) is immiscible and forms a biphasic system. After solvent removal in a vacuum concentrator, residual catalytic activity was measured in HEPES buffer (Figure 5b). As shown in previous experiments (Figure 4a), the lyophilized enzyme converted more substrate after 1 h of reaction than the immobilized form These results indicate that immobilization of PAD in CaBDC does not improve the enzyme's solvent tolerance compared to the lyophilized enzyme. Given the limited stability enhancement observed for PAD and its already well-characterized behavior in organic media, no further investigations were conducted with this system. Instead, subsequent studies focused on CC, which provides a more sensitive and informative model for analyzing enzyme stability in CaBDC under varying process conditions.

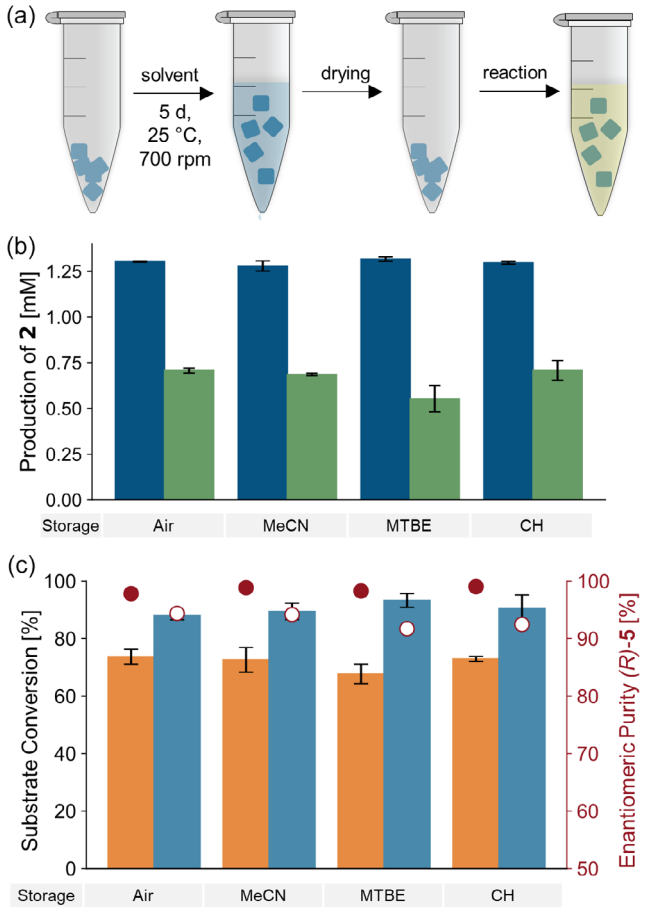

FIGURE 5 | Stability of PAD@CaBDC and CC@CaBDC after incubation in organic solvent. (a) PAD@CaBDC or CC@CaBDC was incubated in organic solvent for 5 days, and after its removal, its activity was investigated in aqueous batch reactions. The same amount of CC was lyophilized and treated identically. (b) Conversions of in batch reactions using 0.3 μM (in regard to the PAD amount) each of lyophilized PAD (blue) or PAD@CaBDC (green) after the treatment from (a) with 1.25 mM **1** in HEPES buffer for 1 h. (c) Substrate conversion (bars) and enantiomeric purity of product **5** (circles) in batch reactions using 5 μM (in regard to the CC amount) each of lyophilized CC (orange) or CC@CaBDC (blue) after the treatment from (a) with 10 mM NaDT, 0.3 mM **3**, and 10 mM **4** in HEPES buffer with 5% MeCN for 4 h under anaerobic conditions. Error bars represent the standard deviation from duplicates.

To further investigate the stabilization of enzymes through encapsulation in MOFs [38, 41–44]. we then conducted experiments on possible improved heat tolerance of CC@CaBDC. As *Rhodothermus marinus* CC originates from a thermohalophilic bacterium [70], it is inherently thermostable, with a calculated melting temperature of 106°C [71]. Indeed, even after heating both soluble CC and CC@CaBDC for 10 min at 120°C followed by 1 min at 150°C, no decrease in catalytic activity was observed in subsequent reactions performed at room temperature (Figure S11). Thus, potential conformational changes in the soluble enzyme do not result in loss of reactivity in the silicon–carbon bond formation reaction. Similarly, 1 h of ultrasound treatment had no negative effect on the activity or enantioselectivity of CC (Figure S12). Overall, CC exhibited remarkable thermal and mechanical robustness, and no additional stabilizing effect of the CaBDC matrix could be detected. These findings underline that enzymes from extremophilic sources may already possess sufficient intrinsic stability to function under harsh process conditions without requiring additional protection through encapsulation.

Next, we examined whether the high intrinsic stability of CC extends to organic solvents and whether encapsulation in CaBDC could further enhance solvent tolerance, following the same procedure as for PAD. For this purpose, CC@CaBDC was incubated for 5 days in MeCN, MTBE, or CH, and then the formation of organosilicon compound **5** in HEPES buffer with 5% MeCN was monitored (Figure 5c). During solvent incubation, CC@CaBDC retained its characteristic orange color, indicating the presence of intact heme cofactor (Figure S13a,b), and XRD confirmed that CaBDC crystallinity remained preserved (Figure S13c). Both lyophilized and immobilized CC showed high substrate conversions and enantiomeric purities comparable to the untreated control (Figure 5b).

When CC@CaBDC samples were washed three times with water before drying, reduced enantiomeric purity at 0.3 mM **3** and lower conversions at 5 mM **3** were observed (Figure S13d). A similar effect was also seen for the sample incubated in air (compare Figures 5c and S13d), suggesting that extensive washing or prolonged water contact can negatively affect catalytic performance.

Repeated washing may promote partial leaching of weakly bound or surface-associated enzyme molecules, thereby reducing the fraction of catalytically competent enzyme. In addition, prolonged aqueous exposure can alter the local microenvironment

within the MOF, for example by modifying ionic strength, disrupting stabilizing interactions between the enzyme and the framework, or leading to oxidation or changes in the redox state, particularly relevant for redox-active enzymes such as CC. Together, these effects can decrease apparent activity. Overall, CC tolerated exposure to MeCN, MTBE, and CH both in its lyophilized and immobilized forms. However, while lyophilized CC completely dissolved in aqueous buffer during catalysis, CC@CaBDC remained as a solid biocatalyst that could be easily recovered and reused by simple centrifugation. Potential stabilizing effects commonly attributed to enzyme@MOF systems, such as enhanced thermal or solvent tolerance, were not observed for the model enzymes and reaction conditions examined in this study. In fact, the more easily prepared soluble enzymes performed mostly better than the enzyme@MOF composites in all tests. These findings emphasize that the protective function of the MOF shell strongly depends on the intrinsic stability of the enzyme. For highly robust enzymes, such as the thermostable and solvent-resistant PAD and CC, encapsulation primarily serves as a means to obtain an insoluble, recoverable catalyst rather than as a stabilizing barrier. In contrast, for more sensitive enzymes, encapsulation may provide significant protection against denaturation and offer a clear advantage for process applications.

The CaBDC framework itself introduces additional parameters that must be considered when designing biocatalytic systems. Partial dissolution of CaBDC in aqueous buffers might lead to linker molecules and metal ions contaminating the final product, while diffusion limitations within its layered structure can influence substrate accessibility and product release. These effects underline the importance of detailed comparative analyses between soluble and immobilized enzymes to obtain mechanistic insights and guide future optimization. Despite these challenges, CaBDC serves as an effective carrier that transforms soluble enzymes into recoverable heterogeneous catalysts, facilitating simple separation and reuse in buffer-containing systems. This feature is particularly valuable for developing long-term biocatalytic processes, including sequential batch or flow operations at preparative scale.

2.5 | Biocatalytic Synthesis of Organosilicon Employing CC@CaBDC in Organic Solvent

Since the stability of both CC and CaBDC in organic solvents had been confirmed, we next investigated the application of CC@CaBDC for catalysis directly in organic media, as previously demonstrated for a lipase encapsulated in CaBDC [72]. Conducting the model reaction in organic solvent requires the enzyme to be supplied already in its reduced state, as the reducing agent commonly employed in CC aqueous reactions (sodium dithionite, NaDT) is not soluble under these conditions. Therefore, CC was first reduced with NaDT in aqueous solution prior to encapsulation via addition of Na_2BDC and 300 mM $CaCl_2$ to form ^{red}CC@CaBDC. The resulting material was then dried to remove residual water, yielding a ready-to-use catalyst for reactions in pure organic solvent (Figure 6a). The distinct red coloration of ^{red}CC@CaBDC compared to CC@CaBDC indicated the successful incorporation of reduced CC, which was confirmed spectrophotometrically by the characteristic absorption band of the reduced heme cofactor in suspension (Figure 6b).

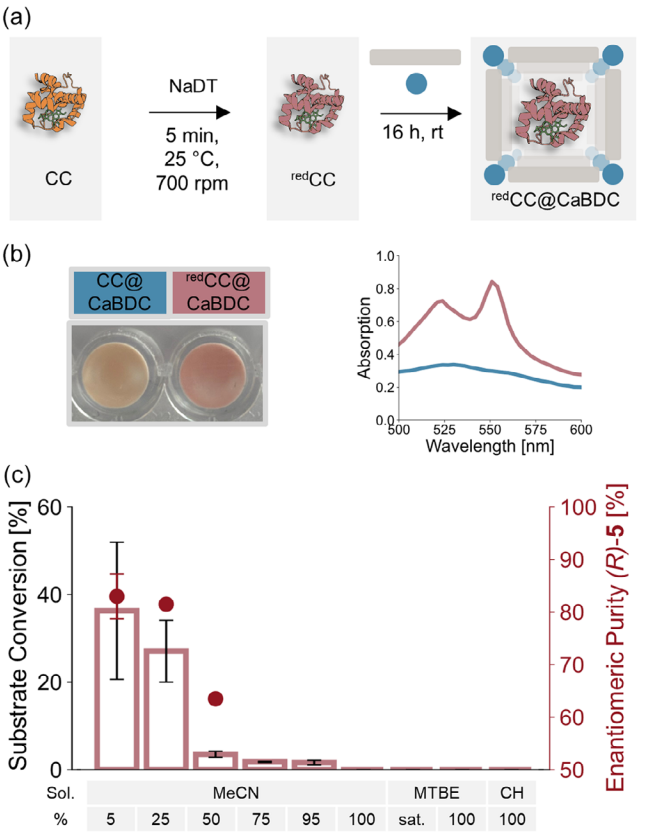

FIGURE 6 | Immobilization of reduced CC in CaBDC-MOF. (a) Reduction of CC using NaDT and subsequent cocrystallization with terephthalate and calcium to form ^{red}CC@CaBDC. (b) Images of CC@CaBDC and ^{red}CC@CaBDC immediately after synthesis and absorption spectrum of a suspension of CC@CaBDC (blue) and ^{red}CC@CaBDC (pink) using a microplate reader. (c) Substrate conversion (bars) and enantiomeric purity of product **5** (circles) in batch reactions by ^{red}CC@CaBDC in HEPES buffer with various proportions of the solvents (sol) MeCN (5%, 25 %, 50%, 75%, and 95%), pure MeCN, MTBE, or CH using 6 μM (in regard to the CC amount) each of ^{red}CC@CaBDC, 10 mM NaDT, 5 mM **3**, and 10 mM **4**. Error bars represent the standard deviation from duplicates.

Microscopic analysis revealed the same butterfly-shaped crystals previously observed for CC@CaBDC (Figure S14a), and XRD confirmed that the crystallinity of CaBDC was maintained after encapsulation (Figure S14b). These results demonstrate the successful immobilization of reduced CC in CaBDC, providing a stable, ready-to-use formulation for catalytic applications in nonaqueous environments.

The catalytic performance of ^{red}CC@CaBDC was evaluated under both anaerobic and aerobic conditions and compared to that of CC@CaBDC. Reactions were conducted in the presence or absence of the reducing agent NaDT (Figure S15). As expected, for CC@CaBDC the addition of NaDT was essential to initiate catalysis, whereas in contrast, ^{red}CC@CaBDC, which already contains the enzyme in its reduced state, achieved a conversion without NaDT close to the conversion upon NaDT addition. Notably, the enantiomeric purity of the product reached 84% in reactions of ^{red}CC@CaBDC without NaDT, representing a clear improvement compared to reactions with CC@CaBDC under standard reducing conditions. Under aerobic conditions,

however, catalytic activity was strongly suppressed in all cases, likely due to competition of molecular oxygen with the substrate for binding to the heme cofactor.

Storage experiments of ^{red}CC@CaBDC for 5 days under anaerobic (red) and aerobic (ox) conditions revealed that molecular oxygen can penetrate the CaBDC pores and oxidize ^{red}CC, leading to decreased activity and a reduced absorption signal at 550 nm (Figure S16). Thus, preservation of the reduced and catalytically active form requires storage under anaerobic conditions, and reactions in organic solvent should likewise be conducted under anoxic environments.

To further assess the performance of ^{red}CC@CaBDC in nonaqueous systems, reactions were tested in three representative organic solvents differing in polarity and water miscibility. While CH's high hydrophobicity precluded any mixing with aqueous buffer, MTBE was tested both in pure form and saturated with water. However, in both cases no product formation was observed (Figure 6c). In contrast, the miscibility of MeCN and HEPES buffer enabled testing of mixed solvent systems with MeCN contents from 5% to 100%. The activity of ^{red}CC@CaBDC gradually decreased with increasing MeCN proportion. Since CC@CaBDC retains activity even after 5 days of storage in MeCN, MTBE, or CH (Figure 5), these results indicate that the lack of reactivity in neat organic solvents could arise from insufficient substrate access rather than enzyme deactivation. It is likely that the substrates remain in the organic phase and fail to penetrate the CaBDC lattice, particularly if residual water within the pores continues to hydrate the enzyme. This hypothesis was confirmed since no significant product formation was detected in biphasic MTBE/HEPES systems for both CC@CaBDC and soluble CC (Figure S17).

In summary, the results demonstrate that encapsulation of reduced CC within CaBDC enables the preparation of a stable, ready-to-use biocatalyst for nonaqueous reactions; however, its activity in pure organic solvents is limited. The observations highlight that, while CaBDC provides an effective microenvironment to preserve enzymatic integrity, achieving efficient catalysis in low-water media will require strategies that enhance substrate diffusion or modify the MOF's internal surface properties. These findings offer important design principles for developing next-generation enzyme@MOF composites tailored for biocatalytic transformations in nonconventional media. The successful reduction of CC with NaDT prior to encapsulation established a practical route to generate ^{red}CC@CaBDC, enabling silicon–carbon bond formation in organic media. We note that, to the best of our knowledge, this work also provides the first demonstration of CC and ^{red}CC encapsulation within a MOF framework, extending MOF-based immobilization to a class of redox-active enzymes previously accessible only through adsorption strategies. However, while the encapsulated enzyme remained catalytically competent, reactivity in pure organic solvents was likely limited by restricted substrate penetration into the MOF lattice. Predicting suitable solvent systems for such hybrid catalysts is therefore not trivial and will require systematic screening of additional solvents, including more polar and protic representatives such as alcohols [73]. In this context, immobilized enzyme composites such as those described here can greatly facilitate such screening efforts, as their solid, reusable nature allows rapid and reproducible testing across different solvent systems. Future work should also address strategies to modify MOF pore surfaces or water content to improve substrate diffusion and compatibility with nonaqueous media. Building on the evaluation strategy established in this study, future efforts can apply similar quantitative and comparative approaches to systematically interrogate enzyme–MOF composites across different enzymes, host frameworks, and reaction conditions. Rather than directly enabling rational material design, such rigorously validated assessments are a prerequisite for distinguishing genuine immobilization effects from artifacts arising from mass-transport limitations, partial framework dissolution, or enzyme release. At the same time, our results underscore that comprehensive characterization and conservative interpretation are essential when assessing the performance of enzyme@MOF composites relative to soluble enzyme formulations. By emphasizing reliable enzyme quantification, critical benchmarking, and explicit consideration of system-specific limitations, this study offers a methodological reference point for future investigations involving CaBDC and related MOF hosts, as well as for applications with other heme-containing carbene transferases [74–76] or decarboxylases.

3 | Conclusion

This study benchmarks enzyme immobilization in CaBDC, showing that in situ encapsulation yields active enzyme@MOF composites across different enzyme classes. Accurate quantification is essential for meaningful evaluation, with SDS–PAGE after MOF dissolution providing a reliable, broadly applicable method. Comparative analysis demonstrated that immobilization does not inherently improve stability but that soluble enzymes can perform better under the investigated conditions.

The benefits of encapsulation depend strongly on enzyme properties: robust enzymes mainly gain recoverability, while less stable ones may benefit from protection. Performance is further influenced by CaBDC-specific limitations, including diffusion barriers and partial framework dissolution, which can obscure true catalytic effects.

Despite these constraints, CaBDC enables reusable heterogeneous biocatalysts and expands immobilization to redox-active enzymes such as ^{red}CC@MOF. However, reduced activity in organic media highlights mass transport challenges and the need for further optimization.

Overall, the work emphasizes that rigorous quantification, direct comparison to soluble systems, and careful consideration of transport and stability effects are critical for reliable benchmarking of enzyme@MOF systems.

4 | Experimental Section

4.1 | PAD Production

PAD was produced heterologous as previously described with minor modifications [25]. The plasmid pET22_PAD-ST-his$_6$, encoding the *Enterococcus* sp.- PAD with a C-terminal SpyTag

and his6 tag, transformed into *E. coli* BL21(DE3). A liquid culture of 100 mL TB-medium containing 100 μg mL^{-1} ampicillin was inoculated from a single colony and cultured at 37°C and 180 rpm for 16 h. Flasks with 2 L of TB-medium (with 100 μg mL^{-1} ampicillin) were inoculated with 30 mL of preculture and incubated at 37°C and 180 rpm until an OD600 of 0.9–1.2 was reached. The cultures were then cooled at 25°C for 30 min and expression was induced by adding 100 μM isopropyl β-D-1-thiogalactopyranoside (IPTG). After incubation for 20 h at 25°C and 180 rpm, the cells were harvested by centrifugation at 10,000 rcf and 4°C for 10 min, resuspended in 40 mL NP_i10 buffer (500 mM NaCl, 50 mM NaH_2PO_4, 10 mM imidazole, pH 8.0) and stored at −80°C until further processing. The cell suspension was thawed at 25°C and subsequently incubated with DNaseI and lysozyme (AppliChem) for 30 min at room temperature. After ultrasonication, cell debris was removed using centrifugation for 1 h at 45,000 rcf and 4°C and the protein-rich supernatant filtered through a 0.45 μm PVDF membrane (Durapore, Steriflip, Millipore). The purification of PAD from the lysate was carried out by fast protein liquid chromatography (FPLC) using the affinity of the his6 tag to a Ni column (5 mL HisTrap FF, Cytiva) installed in an FPLC system (Äkta pure, GE Healthcare). The protein was eluted using a linear gradient from 100% NP_i10 buffer to 100% NP_i500 buffer (500 mM NaCl, 50 mM NaH_2PO_4, 500 mM imidazole, pH 8.0). The collected fractions containing the purified PAD were combined and buffer exchanged to PB (50 mM sodium phosphate, pH 7.4) using centrifugal concentrators (Vivaspin 20, 10,000 MWCO, Sartorius). The concentrated protein solution was aliquoted, frozen in liquid nitrogen and stored at −80°C until use.

4.2 | CC Production

CC was produced heterologous similar to previously described [16]. The plasmid pET22_pelB-CytC(TDE)-his$_6$ [16], encoding the triple mutant TDE of cytochrome C from *Rhodothermus marinus* (CytC(TDE)) [52] with an C-terminal his$_6$ tag, was cotransformed with the cytochrome C maturation plasmid pEC86 (Culture Collection of Switzerland, plasmid no. CCOS 891) [77] into *E. coli* BL21(DE3) using electroporation. *E. coli* cells harboring both plasmids were selected on LB/agar plates containing 100 μg mL^{-1} ampicillin and 30 μg mL^{-1} chloramphenicol overnight at 37°C. A liquid culture of 100 mL TB-medium containing 100 μg mL^{-1} ampicillin and 30 μg mL^{-1} chloramphenicol were generated from a single colony and cultured at 37°C and 180 rpm for 16 h. Using 40 mL of this culture, two flasks with 2 L of TB-medium containing 100 μg mL^{-1} ampicillin and 30 μg mL^{-1} chloramphenicol were inoculated and incubated at 37°C and 180 rpm until an OD_{600} of 1.1 was reached. The cultures were then cooled on ice for 20 min and expression was induced by adding 20 μM isopropyl β-D-1-thiogalactopyranoside (IPTG) and 200 μM 5-aminolevulinic acid. After incubation for 20 h at 20°C and 180 rpm, the cells were harvested by centrifugation at 10,000 rcf and 4°C for 10 min, resuspended in 60 mL NP_i10 buffer (500 mM NaCl, 50 mM NaH_2PO_4, 10 mM imidazole, pH 8.0) and stored at −80°C until further processing. The cell suspension was thawed at 25°C and subsequently incubated with DNaseI and lysozyme (AppliChem) for 30 min at room temperature. After ultrasonication, cell debris was removed using centrifugation for 1 h at 45,000 rcf and 4°C and the protein-rich supernatant filtered through a 0.45 μm PVDF membrane (Durapore, Steriflip, Millipore). The purification of CC from the lysate was carried out by fast protein liquid chromatography (FPLC) using the affinity of the his$_6$ tag to a Ni column (5 mL HisTrap FF, cytiva) installed in an FPLC system (Äkta pure, GE Healthcare). The protein was eluted using a linear gradient from 2% NP_i500 (500 mM NaCl, 50 mM NaH_2PO_4, 500 mM imidazole, pH 8.0) and 98 % NP_i10 to 100% NP_i500 over 10 column volumes. The collected fractions containing the purified CC were combined and buffer exchanged to PB (50 mM sodium phosphate, pH 7.4) using centrifugal concentrators (Vivaspin 20, 5,000 MWCO, Sartorius). The concentrated protein solution was aliquoted, frozen in liquid nitrogen and stored at −80°C until use.

4.3 | Preparation of CaBDC

The synthesis of CaBDC-MOF was performed according to an adapted protocol from the literature [49]. Five hundred microliters of a 600 mM disodium terephthalate (Na_2BDC) solution were mixed with 200 μL of ddH_2O by inverting five times. Three hundred microliters of a 1 M calcium chloride ($CaCl_2$) solution were slowly added dropwise and mixed by vortexing for 5 s at medium speed. The mixture was left at room temperature for 16 h. The next day, the CaBDC formed was washed five times with ddH_2O, for which in each round it was first resuspended, then centrifuged at 11,000 rcf for 3 min, the supernatant was removed, and 1 mL ddH_2O was added. After the last washing step, as much supernatant as possible was removed, and the wet CaBDC was transferred to a weighing paper in a Petri dish under the fume hood, where it dried overnight yielding a white powder.

4.4 | Preparation of Enzyme@CaBDC

Five hundred microliters of a 600 mM Na_2BDC solution were mixed with 150 μL of ddH_2O by inverting five times. Subsequently, 50 μL of a 1 mM enzyme solution (either CC or PAD) in PB or diluted PB (final concentration: 50 μM enzyme) or 195 μL of a 1 mM enzyme solution in water (final concentration: 195 μM enzyme) plus 5 μL of 10x PB buffer were added and mixed again by inverting five times. Three hundred microliters of a 1 M $CaCl_2$ solution were slowly added dropwise and mixed by vortexing for 5 s at medium speed. The mixture was left at room temperature for 16 h, washed five times with ddH_2O and dried overnight, as described above for CaBDC.

4.5 | Preparation of ^{red}CC@CaBDC

The synthesis of ^{red}CC@CaBDC MOF was performed in an anaerobic vinyl chamber. One millimolar CC in PB was reduced with 10 mM sodium dithionite ($Na_2S_2O_4$, NaDT) and incubated for 2 min at 25°C and 700 rpm. Five hundred microliters of a 600 mM Na_2BDC solution were added and mixed by inverting five times. Three hundred microliters of a 1 M $CaCl_2$ solution were slowly added dropwise and mixed by vortexing for 5 s at medium speed. The mixture was left at room temperature for 16 h. The next day, the ^{red}CC@CaBDC formed was washed five times with ddH_2O, for which in each round it was first

resuspended, then briefly centrifuged, the supernatant was removed, and 1 mL ddH_2O was added. After the last washing step, the suspension of ^{red}CC@CaBDC was adjusted to a volume of 1250 and 100 µL of each was distributed in vials. After 10 min, 50 µL of the supernatant was removed and the remaining suspension in the open vial was incubated overnight on a thermoshaker at 25°C and 700 rpm to dry.

4.6 | PAD Activity Measurements

The decarboxylase activity of PAD was measured as previously described [20] with minor modifications. Briefly, 900 µL p-coumaric acid (1.39 mM, **1**) dissolved in HEPES buffer (50 mM, pH 7.4) was incubated at 30°C with 500 rpm shaking for at least 30 min. The reaction was initiated by addition of 100 µL of a 10 mg/mL PAD@CaBDC suspension in HEPES buffer, yielding a final p-coumaric acid concentration of 1.25 mM and a final MOF concentration of 1 mg mL^{-1}. For activity measurements of PAD as soluble enzyme, the reaction was initiated by addition of 100 µL of PAD in HEPES buffer, yielding a final p-coumaric acid concentration of 1.25 mM and a PAD concentration of 0.2 or 0.4 µM (as specified in figure legends). At defined time points, 100 µL of the reaction were sampled and quenched by mixing with 300 µL of a 2:1 (v/v) mixture of acetonitrile and aqueous 0.1% trifluoroacetic acid. The samples were then centrifuged twice and the supernatant was transferred to HPLC vials for further analysis. Measurements were run on $n = 2$ independent MOF syntheses, with $n = 2$ technical replicates run in parallel for each MOF sample.

4.7 | CC Activity Measurements

Reactions employing CC for the formation of silicon-carbon bonds were carried out in an anerobic chamber, as previously described [16]. In a total volume of 400 µL of the chosen reaction medium, soluble or immobilized CC were combined with 10 mM NADT, 0.3, 1.3, or 5 mM ethyl 2-diazopropanoate (**3**) and 10 mM phenyl dimethylsilane (**4**) and incubated for 4 h at 25°C and 700 rpm. The reaction was stopped by adding 1 mL CH and 20 µL of a 20 mM ethyl 2-phenylacetate solution was added as a reference. The mixtures were vortexed for three times for 10 s and centrifuged for 7 min at 13,300 rpm.

Acknowledgments

This work was supported through the Helmholtz program "Materials Systems Engineering" under the topic "Adaptive and Bioinstructive Materials Systems" (43.33.11). A.J.W. is grateful for support by a Kekulé fellowship by Fonds der Chemischen Industrie (FCI). We thank Dr. André Delavault and Astrid Winterhalter for scientific discussion, Dr. Lena Pilz and Dr. Carsten Natzeck for conducting the XRD measurements, and Madleen Richter for experimental help.

Open Access funding enabled and organized by Projekt DEAL.

Funding

This work was supported by the Helmholtz-Gemeinschaft (Grant 43.33.11) and the Fonds der Chemischen Industrie.

Conflicts of Interest

The authors declare no conflicts of interest.

Data Availability Statement

Data is available from the corresponding author upon reasonable request.

References

1. R. A. Sheldon and S. van Pelt, "Enzyme Immobilisation in Biocatalysis: Why, What and How," *Chemical Society Reviews* 42 (2013): 6223–6235, https://doi.org/10.1039/c3cs60075k.

2. K. S. Rabe, J. Muller, M. Skoupi, and C. M. Niemeyer, "Cascades in Compartments: En Route to Machine-Assisted Biotechnology," *Angewandte Chemie-International Edition* 56 (2017): 13574–13589, https://doi.org/10.1002/anie.201703806.

3. R. A. Sheldon, A. Basso, and D. Brady, "New Frontiers in Enzyme Immobilisation: Robust Biocatalysts for a Circular Bio-Based Economy," *Chemical Society Reviews* 50 (2021): 5850–5862, https://doi.org/10.1039/d1cs00015b.

4. J. M. Bolivar, J. M. Woodley, and R. Fernandez-Lafuente, "Is Enzyme Immobilization a Mature Discipline? Some Critical Considerations to Capitalize on the Benefits of Immobilization," *Chemical Society Reviews* 51 (2022): 6251–6290, https://doi.org/10.1039/d2cs00083k.

5. Y. R. Maghraby, R. M. El-Shabasy, A. H. Ibrahim, and H. M. E. Azzazy, "Enzyme Immobilization Technologies and Industrial Applications," *ACS Omega* 8 (2023): 5184, https://doi.org/10.1021/acsomega.2c07560.

6. R. Buller, S. Lutz, R. J. Kazlauskas, R. Snajdrova, J. C. Moore, and U. T. Bornscheuer, "From Nature to Industry: Harnessing Enzymes for Biocatalysis," *Science* 382 (2023): eadh8615, https://doi.org/10.1126/science.adh8615.

7. F. Falcioni, L. Humphreys, R. C. Lloyd, et al., "The Evolving Landscape of Industrial Biocatalysis in Perspective from the ACS Green Chemistry Institute Pharmaceutical Roundtable," *ACS Catalysis* 15 (2025): 10780–10794, https://doi.org/10.1021/acscatal.5c01646.

8. N. Teetz, A. L. Drommershausen, L. Gebele, and D. Holtmann, "Holistic Evaluation of Enzyme Immobilization Processes: A Method for Evaluating the Entire Production Process," *Chemcatchem* 17 (2025): e00699, https://doi.org/10.1002/cctc.202500699.

9. T. Peschke, K. S. Rabe, and C. M. Niemeyer, "Orthogonal Surface Tags for Whole-Cell Biocatalysis," *Angewandte Chemie-International Edition* 56 (2017): 2183–2186, https://doi.org/10.1002/anie.201609590.

10. T. Peschke, M. Skoupi, T. Burgahn, et al., "Self-Immobilizing Fusion Enzymes for Compartmentalized Biocatalysis," *ACS Catalysis* 7 (2017): 7866–7872, https://doi.org/10.1021/acscatal.7b02230.

11. J. Zdarta, A. S. Meyer, T. Jesionowski, and M. Pinelo, "A General Overview of Support Materials for Enzyme Immobilization: Characteristics, Properties, Practical Utility," *Catalysts* 8 (2018): 92, https://doi.org/10.3390/catal8020092.

12. T. Peschke, P. Bitterwolf, S. Hansen, J. Gasmi, K. S. Rabe, and C. M. Niemeyer, "Self-Immobilizing Biocatalysts Maximize Space-Time Yields in Flow Reactors," *Catalysts* 9 (2019): 164, https://doi.org/10.3390/catal9020164.

13. T. Peschke, P. Bitterwolf, K. S. Rabe, and C. M. Niemeyer, "Self-Immobilizing Oxidoreductases for Flow Biocatalysis in Miniaturized Packed-Bed Reactors," *Chemical Engineering & Technology* 42 (2019): 2009–2017, https://doi.org/10.1002/ceat.201900073.

14. R. C. Rodrigues, A. Berenguer-Murcia, D. Carballares, R. Morellon-Sterling, and R. Fernandez-Lafuente, "Stabilization of Enzymes via Immobilization: Multipoint Covalent Attachment and Other Stabilization Strategies," *Biotechnology Advances* 52 (2021): 107821, https://doi.org/10.1016/j.biotechadv.2021.107821.

15. M. Peng, D. L. Siebert, M. K. M. Engqvist, C. M. Niemeyer, and K. S. Rabe, "Modeling-Assisted Design of Thermostable Benzaldehyde Lyases from Rhodococcus Erythropolis for Continuous Production of α-Hydroxy Ketones," *ChemBioChem* 23 (2022), https://doi.org/10.1002/cbic.202100468.

16. S. Gallus, E. Mittmann, A. J. Weber, M. Peng, C. M. Niemeyer, and K. S. Rabe, "An Immobilised Silicon-Carbon Bond-Forming Enzyme for Anaerobic Flow Biocatalysis," *ChemCatChem* 15 (2023): e202300061, https://doi.org/10.1002/cctc.202300061.

17. A. J. Weber, C. Moser, M. A. Martini, et al., "Improving the Long-Term Enantioselectivity of a Silicon-Carbon Bond-Forming Enzyme," *Chemistry - A European Journal* 31 (2025): e202404688, https://doi.org/10.1002/chem.202404688.

18. H. T. Imam, P. C. Marr, and A. C. Marr, "Enzyme Entrapment, Biocatalyst Immobilization without Covalent Attachment," *Green Chemistry* 23 (2021): 4980–5005, https://doi.org/10.1039/d1gc01852c.

19. C. Sicard, "In Situ Enzyme Immobilization by Covalent Organic Frameworks," *Angewandte Chemie-International Edition* 62 (2023), https://doi.org/10.1002/anie.202213405.

20. M. Peng, M. Franzreb, A. J. Weber, P. Lemke, C. M. Niemeyer, and K. S. Rabe, "Enhanced Enzyme Immobilization Using a Novel Agarose-Binding Tag Leads to Improved Flow Reactor Performance," *ChemCatChem* 16 (2024): e202400092, https://doi.org/10.1002/cctc.202400092.

21. R. Kloss, T. Karmainski, V. D. Jäger, et al., "Tailor-Made Catalytically Active Inclusion Bodies for Different Applications in Biocatalysis," *Catalysis Science & Technology* 8 (2018): 5816–5826, https://doi.org/10.1039/c8cy01891j.

22. T. Peschke, P. Bitterwolf, S. Gallus, et al., "Self-Assembling All-Enzyme Hydrogels for Flow Biocatalysis," *Angewandte Chemie-International Edition* 57 (2018): 17028–17032, https://doi.org/10.1002/anie.201810331.

23. P. Bitterwolf, S. Gallus, T. Peschke, et al., "Valency Engineering of Monomeric Enzymes for Self-Assembling Biocatalytic Hydrogels," *Chemical Science* 10 (2019): 9752–9757, https://doi.org/10.1039/c9sc04074a.

24. P. Bitterwolf, F. Ott, K. S. Rabe, and C. M. Niemeyer, "Imine Reductase Based All-Enzyme Hydrogel with Intrinsic Cofactor Regeneration for Flow Biocatalysis," *Micromachines* 10 (2019): 783, https://doi.org/10.3390/mi10110783.

25. E. Mittmann, S. Gallus, P. Bitterwolf, et al., "A Phenolic Acid Decarboxylase-Based All-Enzyme Hydrogel for Flow Reactor Technology," *Micromachines* 10 (2019): 795,https://doi.org/10.3390/mi10120795.

26. V. D. Jäger, R. Lamm, K. Kusters, et al., "Catalytically-Active Inclusion Bodies for Biotechnology-General Concepts, Optimization, and Application," *Applied Microbiology and Biotechnology* 104 (2020): 7313–7329, https://doi.org/10.1007/s00253-020-10760-3.

27. P. Bitterwolf, A. E. Zoheir, J. Hertel, S. Kröll, K. S. Rabe, and C. M. Niemeyer, "Intracellular Assembly of Interacting Enzymes Yields Highly-Active Nanoparticles for Flow Biocatalysis," *Chemistry - A European Journal* 28 (2022), https://doi.org/10.1002/chem.202202157.

28. G. Ölçücü, B. Baumer, K. Küsters, et al., "Catalytically Active Inclusion Bodies?Benchmarking and Application in Flow Chemistry," *ACS Synthetic Biology* 11 (2022): 1881–1896, https://doi.org/10.1021/acssynbio.2c00035.

29. J. S. Hertel, P. Bitterwolf, S. Kroll, et al., "Biocatalytic Foams from Microdroplet-Formulated Self-Assembling Enzymes," *Advanced Materials* 35 (2023): e2303952, https://doi.org/10.1002/adma.202303952.

30. J. S. Hertel, M. A. Martini, M. Stoeckle, A. J. Weber, K. S. Rabe, and C. M. Niemeyer, "Harnessing Non-Covalent Protein-Protein Interaction Domains for Production of Biocatalytic Materials Systems," *Advanced Functional Materials* 36 (2025), https://doi.org/10.1002/adfm.202513931.

31. Y. Jiang, J. X. Zheng, M. N. Wang, et al., "Pros and Cons in Various Immobilization Techniques and Carriers for Enzymes," *Applied Biochemistry and Biotechnology* 196 (2024): 5633, https://doi.org/10.1007/s12010-023-04838-7.

32. M. B. Majewski, A. J. Howarth, P. Li, M. R. Wasielewski, J. T. Hupp, and O. K. Farha, "Enzyme Encapsulation in Metal-Organic Frameworks for Applications in Catalysis," *CrystEngComm* 19 (2017): 4082–4091, https://doi.org/10.1039/c7ce00022g.

33. Y. M. Feng, Y. Xu, S. C. Liu, et al., "Recent Advances in Enzyme Immobilization Based on Novel Porous Framework Materials and Its Applications in Biosensing," *Coordination Chemistry Reviews* 459 (2022): 214414, https://doi.org/10.1016/j.ccr.2022.214414.

34. Z. H. Wu, H. T. Shan, Y. S. Jiao, et al., "Covalent Organic Networks for In Situ Entrapment of Enzymes with Superior Robustness and Durability," *Chemical Engineering Journal* 450 (2022): 138446, https://doi.org/10.1016/j.cej.2022.138446.

35. O. M. Yaghi, G. M. Li, and H. L. Li, "Selective Binding and Removal of Guests in a Microporous Metal-Organic Framework," *Nature* 378 (1995): 703–706, https://doi.org/10.1038/378703a0.

36. L. Jiao, J. Y. R. Seow, W. S. Skinner, Z. U. Wang, and H. L. Jiang, "Metal-Organic Frameworks: Structures and Functional Applications," *Materials Today* 27 (2019): 43–68, https://doi.org/10.1016/j.mattod.2018.10.038.

37. J. N. Yang, O. Zaremba, J. Andreo, H. Gröger, and S. Wuttke, "Unravelling the Potential of Crude Enzyme Extracts for Biocatalyst Entrapment in Metal-Organic Frameworks," *ACS Nano* 19 (2025): 14817–14828, https://doi.org/10.1021/acsnano.4c18266.

38. W. Liang, P. Wied, F. Carraro, et al., "Metal-Organic Framework-Based Enzyme Biocomposites," *Chemical Reviews* 121 (2021): 1077–1129, https://doi.org/10.1021/acs.chemrev.0c01029.

39. D. Jordahl, Z. Armstrong, Q. Li, et al., "Expanding the "Library" of Metal-Organic Frameworks for Enzyme Biomineralization," *ACS Applied Materials & Interfaces* 14 (2022): 51619–51629, https://doi.org/10.1021/acsami.2c12998.

40. J. Rogacka and K. Labus, "Metal-Organic Frameworks as Highly Effective Platforms for Enzyme Immobilization-Current Developments and Future Perspectives," *Brazilian Journal of Chemical Engineering* 42 (2024): 1273, https://doi.org/10.1007/s43153-024-00513-4.

41. S. Huang, X. Kou, J. Shen, G. Chen, and G. Ouyang, "Armor-Plating" Enzymes with Metal-Organic Frameworks (MOFs)," *Angewandte Chemie-International Edition* 59 (2020): 8786–8798, https://doi.org/10.1002/anie.201916474.

42. X. Wu, C. Yang, and J. Ge, "Green Synthesis of Enzyme/Metal-Organic Framework Composites with High Stability in Protein Denaturing Solvents," *Bioresources and Bioprocessing* 4 (2017): 24, https://doi.org/10.1186/s40643-017-0154-8.

43. S. S. Nadar and V. K. Rathod, "Facile Synthesis of Glucoamylase Embedded Metal-Organic Frameworks (glucoamylase-MOF) with Enhanced Stability," *International Journal of Biological Macromolecules* 95 (2017): 511–519, https://doi.org/10.1016/j.ijbiomac.2016.11.084.

44. L. Wang, W. J. Zhi, D. S. Lan, Y. Wang, J. Han, and Y. Wang, "HRP@ZIF-8/DNA Hybrids: Functionality Integration of ZIF-8 via Biomineralization and Surface Absorption," *ACS Sustainable Chemistry & Engineering* 7 (2019): 14611–14620, https://doi.org/10.1021/acssuschemeng.9b02348.

45. R. Greifenstein, T. Ballweg, T. Hashem, et al., "MOF-Hosted Enzymes for Continuous Flow Catalysis in Aqueous and Organic Solvents," *Angewandte Chemie-International Edition* 61 (2022), https://doi.org/10.1002/anie.202117144.

46. Y. J. Du, X. T. Jia, L. Zhong, et al., "Metal-Organic Frameworks with Different Dimensionalities: An Ideal Host Platform for Enzyme@MOF Composites," *Coordination Chemistry Reviews* 454 (2022): 214327, https://doi.org/10.1016/j.ccr.2021.214327.

47. S. H. Dale and M. R. J. Elsegood, "Catena-Poly[[diaquacalcium(II)]-μ3-Terephthalato-μ2-Aqua] at 150 K," *Acta Crystallographica Section E:*

Crystallographic Communications 59 (2003): M586–M587, https://doi.org/10.1107/S1600536803015071.

48. J. Farmakes, I. Schuster, A. Overby, et al., "Enzyme Immobilization on Graphite Oxide (GO) Surface via One-Pot Synthesis of GO/Metal-Organic Framework Composites for Large-Substrate Biocatalysis," *ACS Applied Materials & Interfaces* 12 (2020): 23119–23126, https://doi.org/10.1021/acsami.0c04101.

49. Q. B. Li, Y. X. Pan, H. Li, et al., "Size-Tunable Metal-Organic Framework-Coated Magnetic Nanoparticles for Enzyme Encapsulation and Large-Substrate Biocatalysis," *ACS Applied Materials & Interfaces* 12 (2020): 41794–41801, https://doi.org/10.1021/acsami.0c13148.

50. Y. Pan, Q. Li, H. Li, et al., "A General Ca-MOM Platform with Enhanced Acid-Base Stability for Enzyme Biocatalysis," *Chem Catalysis* 1 (2021): 146–161.

51. W. Gu, X. M. Li, J. W. Huang, et al., "Cloning, Sequencing, and Overexpression in *Escherichia coli* of the *Enterobacter* sp. Px6-4 Gene for Ferulic Acid Decarboxylase," *Applied Microbiology and Biotechnology* 89 (2011): 1797–1805, https://doi.org/10.1007/s00253-010-2978-4.

52. S. B. Kan, R. D. Lewis, K. Chen, and F. H. Arnold, "Directed Evolution of Cytochrome c for Carbon-Silicon Bond Formation: Bringing Silicon to Life," *Science* 354 (2016): 1048–1051, https://doi.org/10.1126/science.aah6219.

53. C. Wuensch, T. Pavkov-Keller, G. Steinkellner, et al., "Regioselective Enzymatic Beta-Carboxylation of Para-Hydroxy- Styrene Derivatives Catalyzed by Phenolic Acid Decarboxylases," *Advanced Synthesis & Catalysis* 357 (2015): 1909–1918, https://doi.org/10.1002/adsc.201401028.

54. R. D. Lewis, M. Garcia-Borras, M. J. Chalkley, et al., "Catalytic Iron-Carbene Intermediate Revealed in a Cytochrome c Carbene Transferase," *Proceedings of the National Academy of Sciences of the United States of America* 115 (2018): 7308–7313, https://doi.org/10.1073/pnas.1807027115.

55. F. Lyu, Y. Zhang, R. N. Zare, J. Ge, and Z. Liu, "One-Pot Synthesis of Protein-Embedded Metal-Organic Frameworks with Enhanced Biological Activities," *Nano Letters* 14 (2014): 5761–5765, https://doi.org/10.1021/nl5026419.

56. H. Abdelhamid, "Biointerface between ZIF-8 and Biomolecules and Their Applications," *Biointerface Research in Applied Chemistry* 11 (2021): 8283–8297, https://doi.org/10.33263/BRIAC111.82838297.

57. K. Yang, G. N. Chen, L. Wang, et al., "Zeolitic-Imidazolate Framework (ZIF-8)-Based Immobilized Multi-Enzymes Integrated with a Colorimetric Sensor for Cholesterol Assay," *New Journal of Chemistry* 47 (2023): 4103–4112, https://doi.org/10.1039/d2nj05747f.

58. W. B. Liang, H. S. Xu, F. Carraro, et al., "Enhanced Activity of Enzymes Encapsulated in Hydrophilic Metal-Organic Frameworks," *Journal of the American Chemical Society* 141 (2019): 2348–2355, https://doi.org/10.1021/jacs.8b10302.

59. H. Peng, W. G. Dong, Q. W. Chen, et al., "Encapsulation of Nitrilase in Zeolitic Imidazolate Framework-90 to Improve Its Stability and Reusability," *Applied Biochemistry and Biotechnology* 194 (2022): 3527–3540, https://doi.org/10.1007/s12010-022-03890-z.

60. X. L. Sun, J. H. Hu, Y. F. Zhou, et al., "Innovative Strategy of ZIF-90 for Co-Immobilization of Whole Cells and Enzymes in Biocatalytic-Phenyllactic Acid Synthesis," *International Journal of Biological Macromolecules* 283 (2024): 137735, https://doi.org/10.1016/j.ijbiomac.2024.137735.

61. V. Gascón, E. Castro-Miguel, M. Díaz-García, R. M. Blanco, and M. Sanchez-Sanchez, "In Situ and Post-Synthesis Immobilization of Enzymes on Nanocrystalline MOF Platforms to Yield Active Biocatalysts," *Journal of Chemical Technology and Biotechnology* 92 (2017): 2583–2593, https://doi.org/10.1002/jctb.5274.

62. Z. Nowroozi-Nejad, B. Bahramian, and S. Hosseinkhani, "A Fast and Efficient Stabilization of Firefly Luciferase on MIL-53(Al) via Surface Adsorption Mechanism," *Research on Chemical Intermediates* 45 (2019): 2489–2501, https://doi.org/10.1007/s11164-019-03748-w.

63. X. Peng, C. X. Pei, E. W. Qian, Y. G. Du, and J. J. Li, "Co-Immobilization of a Bi-Enzymatic Cascade into Hierarchically Porous MIL-53 for Efficient 6′-Sialyllactose Production," *Nanoscale* 16 (2024): 14932–14939, https://doi.org/10.1039/d4nr01775g.

64. X. L. Wang, J. F. Shi, S. H. Zhang, et al., "MOF-Templated rough, Ultrathin Inorganic Microcapsules for Enzyme Immobilization," *Journal of Materials Chemistry B* 3 (2015): 6587–6598, https://doi.org/10.1039/c5tb00870k.

65. W. C. Zhou, S. Begum, Z. B. Wang, et al., "High Antimicrobial Activity of Metal-Organic Framework-Templated Porphyrin Polymer Thin Films," *ACS Applied Materials & Interfaces* 10 (2018): 1528–1533, https://doi.org/10.1021/acsami.7b14866.

66. G. S. Chen, X. X. Kou, S. M. Huang, et al., "Modulating the Biofunctionality of Metal-Organic Framework-Encapsulated Enzymes through Controllable Embedding Patterns," *Angewandte Chemie-International Edition* 59 (2020): 2867–2874, https://doi.org/10.1002/anie.201913231.

67. D. Buzek, S. Adamec, K. Lang, and J. Demel, "Metal-Organic Frameworks vs. Buffers: Case Study of UiO-66 Stability," *Inorganic Chemistry Frontiers* 8 (2021): 720–734, https://doi.org/10.1039/d0qi00973c.

68. P. Petermeier, J. P. Bittner, S. Müller, E. Byström, and S. Kara, "Design of a Green Chemoenzymatic Cascade for Scalable Synthesis of Bio-Based Styrene Alternatives," *Green Chemistry* 24 (2022): 6889–6899, https://doi.org/10.1039/d2gc01629j.

69. K. Faber, *Biotransformations in Organic Chemistry*, 7thed. (Springer, 2018).

70. G. A. Alfredsson, J. K. Kristjansson, S. Hjorleifsdottir, and K. O. Stetter, "*Rhodothermus-Marinus*, Gen-Nov, Sp-Nov, a Thermophilic, Halophilic Bacterium from Submarine Hot Springs in Iceland," *Journal of General Microbiology* 134 (1988): 299–306.

71. M. Stelter, A. M. Melo, M. M. Pereira, et al., "A Novel Type of Monoheme Cytochrome c: Biochemical and Structural Characterization at 1.23 A Resolution of *Rhodothermus marinus* Cytochrome c," *Biochemistry* 47 (2008): 11953–11963, https://doi.org/10.1021/bi800999g.

72. W. J. Li, Y. M. Li, H. Ren, C. Y. Ji, and L. Cheng, "Improving the Bioactivity and Stability of Embedded Enzymes by Covalent Organic Frameworks," *ACS Applied Materials & Interfaces* 15 (2023): 43580–43590, https://doi.org/10.1021/acsami.3c09459.

73. A. Delavault, K. Ochsenreither, and C. Syldatk, "Intensification of Biocatalytic Processes by Using Alternative Reaction Media," *Physical Sciences Reviews* 9 (2024): 2875–2897, https://doi.org/10.1515/psr-2022-0104.

74. Z. Liu and F. H. Arnold, "New-to-Nature Chemistry from Old Protein Machinery: Carbene and Nitrene Transferases," *Current Opinion in Biotechnology* 69 (2021): 43–51, https://doi.org/10.1016/j.copbio.2020.12.005.

75. Y. Yang and F. H. Arnold, "Navigating the Unnatural Reaction Space: Directed Evolution of Heme Proteins for Selective Carbene and Nitrene Transfer," *Accounts of Chemical Research* 54 (2021): 1209–1225, https://doi.org/10.1021/acs.accounts.0c00591.

76. P. Kaur and V. Tyagi, "Recent Advances in Iron-Catalyzed Chemical and Enzymatic Carbene-Transfer Reactions," *Advanced Synthesis & Catalysis* 363 (2021): 877–905, https://doi.org/10.1002/adsc.202001158.

77. E. Arslan, H. Schulz, R. Zufferey, P. Künzler, and L. Thöny-Meyer, "Overproduction of the *Bradyrhizobium japonicum* c-Type Cytochrome Subunits of the cbb3 Oxidase in *Escherichia coli*," *Biochemical and Biophysical Research Communications* 251 (1998): 744–747, https://doi.org/10.1006/bbrc.1998.9549.

Supporting Information

Additional supporting information can be found online in the Supporting Information section.